A trade-off between model resolution and variance with selected Rayleigh-wave data

Jianghai Xia, Richard D. Miller, Kansas Geological Survey, The University of Kansas*
Yixian Xu, State Key Laboratory of Geological Processes and Mineral Resources, China University of Geosciences

Summary

Inversion of multimode surface-wave data is of increasing interest in the near-surface geophysics community. For a given near-surface geophysical problem, it is essential to understand how well the data, calculated according to a layered-earth model, might match the observed data. A data-resolution matrix is a function of the data kernel (determined by a geophysical model and a priori information applied to the problem), not the data. A data-resolution matrix of high-frequency (≥ 2 Hz) Rayleigh-wave phase velocities, therefore, offers a quantitative tool for designing field surveys and predicting the match between calculated and observed data. First, we employed a data-resolution matrix to select data that would be well predicted and to explain advantages of incorporating higher modes in inversion. The resulting discussion using the data-resolution matrix provides insight into the process of inverting Rayleigh-wave phase velocities with higher mode data to estimate S-wave velocity structure. Discussion also suggested that each near-surface geophysical target can only be resolved using Rayleigh-wave phase velocities within specific frequency ranges, and higher mode data are normally more accurately predicted than fundamental mode data because of restrictions on the data kernel for the inversion system. Second, we obtained an optimal damping vector in a vicinity of an inverted model by the singular value decomposition of a trade-off function of model resolution and variance. In the end of the paper, we used a real-world example to demonstrate that selected data with the data-resolution matrix can provide better inversion results and to explain with the data-resolution matrix why incorporating higher mode data in inversion can provide better results. We also calculated model-resolution matrices of these examples to show the potential of increasing model resolution with selected surface-wave data. With the optimal damping vector, we can improve and assess an inverted model obtained by a damped least-square method.

Introduction

Elastic properties of near-surface materials and their influence on seismic-wave propagation are of fundamental interest in ground water, engineering, and environmental studies. Shear (S)-wave velocities can be estimated by inverting dispersive surface-wave phase velocities (Rayleigh and/or Love) (e.g., Dorman and Ewing, 1962; Aki and Richards, 1980, p. 664). Surface-wave techniques have been given increasingly more attention by the near-surface geophysics community with application to a variety of near-surface geological and geophysical problems. Errors in S-wave velocities obtained using the surface wave techniques (e.g., Song et al., 1989) are 15% or less and random when compared with direct borehole measurements (Xia et al., 1999, 2002a). Other studies associated with inversion of surface-wave data include delineation of bedrock (Miller et al., 1999), near-surface quality factors (Q) (Xia et al., 2002b), a pitfall using shear-wave refraction surveying (Xia et al., 2002c), detection of voids (Xia et al., 2004), joint inversion of refractions and surface waves (Ivanov et al., 2006), estimation of S-wave velocities for a continuous earth model (Xia et al., 2006), discussion of surface-wave inversion with a high-velocity-layer intrusion model (Calderón-Macías and Luke, 2007), and a low-velocity-layer intrusion model (Lu et al., 2007; Liang et al., in press).

Inversion of Rayleigh waves is a key step to leading to previously mentioned studies. For a given near-surface geophysical problem, it is essential to understand how well the data, calculated according to a layered-earth model, might match the observed data. It is important to recognize that a match may only be possible for data within a certain frequency range or at specific frequencies because the sensitivity of Rayleigh-wave phase velocities due to changes in S-wave velocities varies with frequency. It is also critical to estimate error in inverse solutions by a damped least-square method. Most surface-wave researchers are aware that accuracy of inverted S-wave velocities can be significantly improved with the incorporation of higher mode data (Xia et al., 2003; Beaty et al., 2002; Luo et al., 2007; Liang et al., in press). Xia et al. (2003) identified two quite significant higher mode properties through analysis of the Jacobian matrix populated with high-frequency Rayleigh-wave data. First, for fundamental and higher mode Rayleigh wave data with the same wavelength, higher mode Rayleigh waves penetrate deeper than the fundamental mode. Second, higher mode data increase resolution of inverted S-wave velocities. We also noticed that data at certain frequencies within the same mode are more important than others in resolving S-wave velocities.

In this paper, we will show how the data-resolution matrix can reveal the intrinsic properties of surface-wave inversion. We will use a real data example to show why higher mode data can generally be more accurately predicted than fundamental mode data and will demonstrate that more accurate S-wave velocities can be obtained using Rayleigh-wave data inversion with

only predictable phase velocities that are selected based on data-resolution matrix. Finally, we will determine a trade-off between model resolution and covariance, which provides a model with good resolution and relatively low variance.

Data-resolution matrix and model-resolution matrix

Near-surface S-wave velocities can be estimated by inverting phase velocities of high-frequency Rayleigh waves (Xia et al., 1999, 2003, and 2006). Near-surface quality factors (Q) can also be determined by inverting attenuation coefficients of Rayleigh waves (Xia et al., 2002b). Both estimation techniques are based on the overdetermined system $\mathbf{Gm}^{true} = \mathbf{d}^{obs}$, where $\mathbf{G}$ is an m $\times$ n matrix (m > n in both cases, m denotes the number of data and n the number of unknowns), and $\mathbf{m}^{true}$ and $\mathbf{d}^{obs}$ are model and observed data vectors, respectively. $\mathbf{G}$ stands for a data kernel that embodies $\mathbf{m}^{true}$ and includes the experimental geometry. Letting $\mathbf{H}$ be a generalized inverse of $\mathbf{G}$, we can estimate model $\mathbf{m}^{est} = \mathbf{Hd}^{obs}$. With these two equations, we obtain $\mathbf{d}^{pre} = \mathbf{Gm}^{est} = \mathbf{G}[\mathbf{Hd}^{obs}] = [\mathbf{GH}]\mathbf{d}^{obs} = \mathbf{Nd}^{obs}$. Matrix $\mathbf{N} = \mathbf{GH}$ is the m $\times$ m data-resolution matrix (Minster et al., 1974). The data-resolution matrix is only determined by the data kernel and any a priori information added to the problem. Each predicted datum is a weighted average of observed data with a row vector of $\mathbf{N}$ as a weighting function. The generalized inverse of the least-square solution is $\mathbf{H} = [\mathbf{G}^T\mathbf{G} + \lambda\mathbf{I}]^{-1}\mathbf{G}^T$ (Marquardt, 1965), where $\mathbf{G}$ is the Jacobian matrix of the model with respect to S-wave velocity, λ is a damping factor, and $\mathbf{I}$ is the unit matrix. So the data-resolution matrix is

$$\mathbf{N} = \mathbf{G}[\mathbf{G}^T\mathbf{G} + \lambda\mathbf{I}]^{-1}\mathbf{G}^T \approx \mathbf{G}[\mathbf{G}^T\mathbf{G}]^{-1}\mathbf{G}^T, \quad (1)$$

when iterations converge to a local or global minimum, the damping factor λ approaches to zero (Xia et al., 2005).

On the other hand, with the first two equations in the last paragraph, we obtain the model-resolution matrix (Wiggins, 1972) for an overdetermined system (m > n) with the damped least square method $\mathbf{m}^{est} = \mathbf{HGm}^{true} = [\mathbf{G}^T\mathbf{G} + \lambda\mathbf{I}]^{-1}\mathbf{G}^T\mathbf{Gm}^{true} = \mathbf{Rm}^{true}$, where the model-resolution matrix $\mathbf{R}$ is an n $\times$ n matrix

$$\mathbf{R} = [\mathbf{G}^T\mathbf{G} + \lambda\mathbf{I}]^{-1}\mathbf{G}^T\mathbf{G}. \quad (2)$$

A trade-off between model resolution and variance

For a linear system, if data are assumed to be uncorrelated, the unit covariance matrix of an inverted model is $\mathbf{C} = \mathbf{HH}^T$ (Menke, 1984). Therefore, the unit covariance matrix of a damped least-square solution is

$$\mathbf{C} = \mathbf{HH}^T = [\mathbf{G}^T\mathbf{G} + \lambda\mathbf{I}]^{-1}\mathbf{G}^T([\mathbf{G}^T\mathbf{G} + \lambda\mathbf{I}]^{-1}\mathbf{G}^T)^T. \quad (3)$$

With the singular value decomposition $\mathbf{G} = \mathbf{U}\Lambda\mathbf{V}^T$, where $\mathbf{U}$ and $\mathbf{V}$ are a semi-orthogonal and an orthogonal matrix, respectively, and Λ is a diagonal matrix that holds singular values Λ_i, i = 1, 2, …, n (Golub and Reinsch, 1970), and $\mathbf{G}^T\mathbf{G} + \lambda\mathbf{I} = \mathbf{V}(\Lambda^2 + \lambda\mathbf{I})\mathbf{V}^T$. The damping factor can be determined by a trade-off curve between resolution and variance of a model (Menke, 1984), which will minimize the following function:

$$\Phi = (1 - \alpha)\mathbf{C} + \alpha(\mathbf{I} - \mathbf{R}) = \mathbf{V}\{(1 - \alpha)\Lambda^2[\Lambda^2 + \lambda\mathbf{I}]^{-2} + \alpha(\mathbf{I} - \Lambda^2[\Lambda^2 + \lambda\mathbf{I}]^{-1})\}\mathbf{V}^T, \quad (4)$$

where λ and α are normally a damping factor (scalar) and a weighting factor (scalar), respectively. They can be vectors as we discuss in the followings. Φ is a function of λ and α. The matrix in the parenthesis {} is a diagonal matrix with the ith element

$$\phi_i = (1 - \alpha_i)\Lambda_i^2[\Lambda_i^2 + \lambda_i]^{-2} + \alpha_i(1 - \Lambda_i^2[\Lambda_i^2 + \lambda_i]^{-1}), \quad (5)$$

where λ_i and α_i are the ith element of the damping vector and of the weighing vector, respectively. To minimize the sum of diagonal elements of Φ, we only need to minimize each coefficient ϕ_i (Equation 5). Therefore, we find the following λ_i and α_i that minimize ϕ_i,

$$\lambda_i = 0.5(\sqrt{\Lambda_i^4 + 4\Lambda_i^2} - \Lambda_i^2) \text{ and } \alpha_i = 2(2 + \Lambda_i^2 + \lambda_i)^{-1}. \quad (6)$$

We can show $0 < \lambda_i < 1$ with relationships of three sides of a right triangle, two sides the right angle of which are Λ_i^2 and $2\Lambda_i$. In practice, we can estimate a model standard deviation with the following formula,

$$\Delta m_i = \Delta d\sqrt{\sum_{j=1}^{n}\gamma_j v_{ij}^2}, \quad (7)$$

where Δm_i is the ith element of the model standard deviation $\Delta\mathbf{m}$, Δd is the data standard deviation, which could be replaced by a threshold of terminating iterations, $\gamma_j = \Lambda_j^2[\Lambda_j^2 + \lambda_j]^{-2}$, and $\mathbf{V}_{ij}$ is the element of matrix $\mathbf{V}$ at the ith row and the jth column.

An example

Data were acquired in San Jose, California (Figure 1a) that included well-defined second modes in the frequency-velocity domain (Figure 1b) (Xia et al., 2003). A 14-layer model with layer thicknesses of 1 m was used to invert the Rayleigh-wave data. We

calculated the data-resolution matrix of the multi-layer model with selected 35 data points from different frequencies up to the second mode (Figure 2) to show how well each datum and each mode could be predicted. The row number of matrix **N** associated with the data is listed in Table 1. If there are the same frequencies in consecutive rows, the second indicates the second mode.

Table 1. Order of data points in the data-resolution matrix of the San Jose example.

Row	1	2	3	4	5	6	7	8	9	10	11	12	13	14	15	16	17	
Freq. (Hz)	7	8	9	10	11	12	13	14	15	16	17	18	19	20	20	21	21	
Row	18	19	20	21	22	23	24	25	26	27	28	29	30	31	32	33	34	35
Freq. (Hz)	22	22	23	23	24	24	25	25	26	26	27	27	28	28	29	29	30	30

The diagonal elements of this data-resolution matrix of the 14-layer model (Figure 2) possess the highest values of each row vector, which means measured data can normally be predicted. We noticed based on the data-resolution matrix that the first seven data from frequencies 7 to 13 Hz (rows 1 to 7) are critical to defining S-wave velocities. Second mode data with frequencies greater than 20 Hz (rows 15, 17, 19, 21, 23, 25, 27, 29, 31, 33, and 35) possess higher diagonal values than fundamental mode data at the same frequencies. For example, the fundamental mode datum at 21 Hz is poorly predicted due to its broad weighting function, but the second mode datum at the same frequency can be well predicted because of its spike-like weighting function.

We inverted 16 data selected based on Figure 2 (the data-resolution matrix) that possess diagonal values of 0.45 and higher (Table 2 in bold). Sixteen data are near the minimum number of data necessary to solve the problem with 14 unknowns. The initial model was the same as the one used in Xia et al. (2003) with the same initial damping factor (λ_0 = 1). We showed inverted results from the selected data and inverted results from multi-mode data (28 data points with the fundamental mode data up to 23 Hz, Xia et al., 2003) in Figure 3 with the best-inverted model that was obtained from "error-free" data (labeled "true" in Figure 3). Overall, inversion results of the 16 selected data are closer to the "true" model than results from multi-mode data (Xia et al., 2003).

Table 2. Data selected in inversion in bold (the San Jose example, Xia et al., 2003).

Row	1	2	3	4	5	6	7	8	9	10	11	12	13	14	15	16	17	
Freq. (Hz)	**7**	**8**	**9**	**10**	**11**	**12**	**13**	14	**15**	**16**	17	18	19	20	**20**	21	**21**	
Row	18	19	20	21	22	23	24	25	26	27	28	29	30	31	32	33	34	35
Freq. (Hz)	22	**22**	23	**23**	24	24	25	**25**	26	26	27	27	28	**28**	29	29	30	**30**

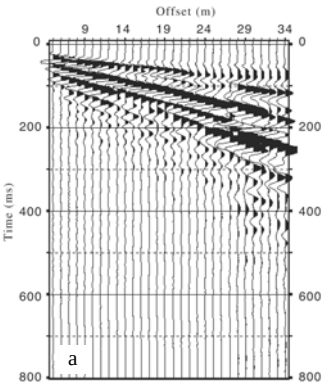

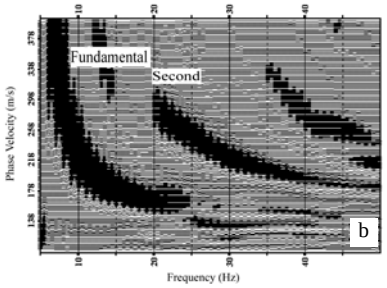

Figure 1. An example from San Jose, California (Xia et al., 2003). a) Raw surface-wave data and b) their image in the frequency-velocity domain.

The inversion of the 28-data set was converged to the model denoted by squares (Figure 3) with $\lambda = 10^{-1}$ (Xia et al., 2003). The corresponding model-resolution matrix calculated using Equation 2 was shown in Figure 4a. The inversion of 16 selected data was converged to the model denoted by triangles (Figure 3) with $\lambda = 10^{-3}$. The corresponding model-resolution matrix calculated using Equation 2 was shown in Figure 4b. It is clear that the model inverted from 16 selected data possesses a higher model resolution overall, especially for layers 11, 12, and 13.

Figure 4b shows the inverted model from 16 selected data possesses higher model resolution but the model also has higher variance (diagonal elements of the covariance matrix, Table 3). As we

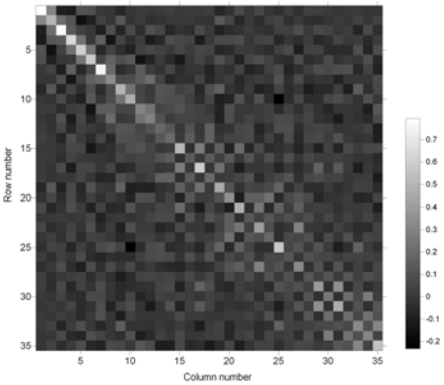

Figure 2. The data-resolution matrix of the San Jose example (Table 1).

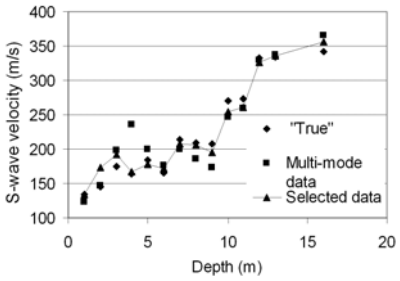

Figure 3. Inversion results of the San Jose example. Model "True" was obtained from inverting "error-free" data and "Multi-mode data" was the inverted model from 28 multi-mode data (Xia et al., 2003). "Selected data" was the inverted model from 16 data selected based on data-resolution functions.

discussed in the previous section, an extra iteration starting from this model with damping factors and weighting factors determined by Equation 6 (Table 4) can produce a trade-off model between model resolution and variance (Table 5). Model variance is dramatically reduced at the cost of reduce model resolution. The Euler distance between the trade-off model and the model from selected data (triangles in Figure 3) is 2.425 m/s. With Equation 7, we can estimate a standard deviation in the trade-off model if assuming data are uncorrelated and using the threshold of terminating iterations (5.8 m/s) as the standard deviation of data. The maximum standard deviation of $\pm$ 20 m/s is associated with layer 14 (Figure 5).

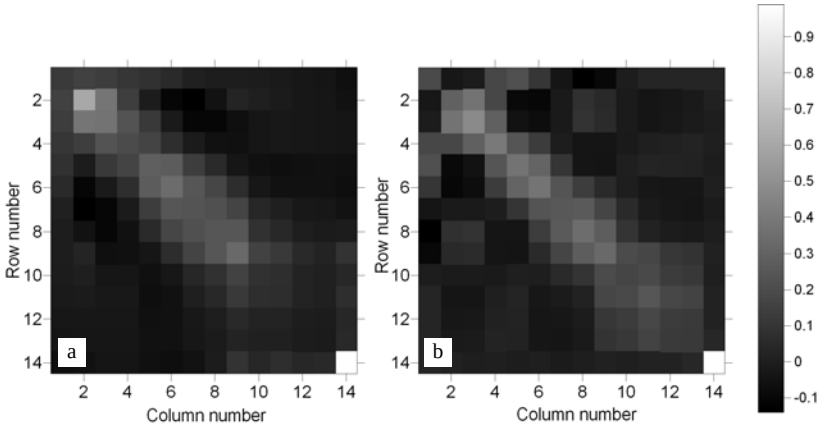

Figure 4. The model resolution matrixes of the San Jose example (Xia et al., 2003) based on a) the inverted model from 28 data and on b) the inverted model from 16 selected data associated with the corresponding diagonal values of the data resolution matrix of 0.45 and higher.

Conclusions

We employed the data-resolution matrix to show that, in general, higher mode data are normally more accurately predicted than lower mode data. This characteristic explains why inversion of higher mode data normally results in more accurate models. The example demonstrated that the inverted model from data selected based on the data-resolution matrix is better than the model inverted from multi-mode data that were not selected. The model-resolution matrix of the example also suggested that inverted results from selected surface-wave data might possess higher model resolution. Data can be selected based on the data-resolution matrix of a good initial model. Because the data-resolution matrix is only related to the data kernel and a priori information applied to the problem not the function of data (Menke, 1984), we can use the data-resolution matrix to establish requirements for a given problem, such as data existence in specific frequency ranges. After finding a solution with a damped least-square method, an extra iteration, with the optimal damping vector that we derived, can be performed to find a trade-off between model resolution and model covariance. The unit covariance matrix with the optimal vector provides a tool of assessment of inverted models obtained using a damped least-square method.

Table 3. Model resolution and variance (diagonal elements of **R** and **C** of the model in triangles in Figure 3).

Layer #	1	2	3	4	5	6	7	8	9	10	11	12	13	14
Resolution	0.30	0.408	0.55	0.49	0.46	0.46	0.36	0.44	0.43	0.29	0.34	0.26	0.24	0.99
Variance	0.17	0.71	5.83	12.9	145	394	308	373	362	244	290	220	202	838

Table 4. Damping factors and weighting factors for the trade-off model (Figure 5).

Layer #	1	2	3	4	5	6	7	8	9	10	11	12	13	14
Damping	0.72	0.52	0.26	0.18	0.05	0.01	0.01	0.01	0.01	0.01	0.01	0.01	0.01	0.01
Weighting	0.44	0.65	0.85	0.90	0.98	0.99	0.99	0.99	0.99	0.99	0.99	0.99	0.99	0.99

Table5. Model resolution and variance (diagonal elements of **R** and **C** of the trade-off model).

Layer #	1	2	3	4	5	6	7	8	9	10	11	12	13	14
Resolution	0.03	0.05	0.08	0.12	0.11	0.14	0.09	0.09	0.09	0.03	0.03	0.02	0.02	0.34
Variance	0.01	0.03	0.13	0.31	1.22	5.23	3.33	3.48	3.37	1.28	1.14	0.63	0.54	12.6

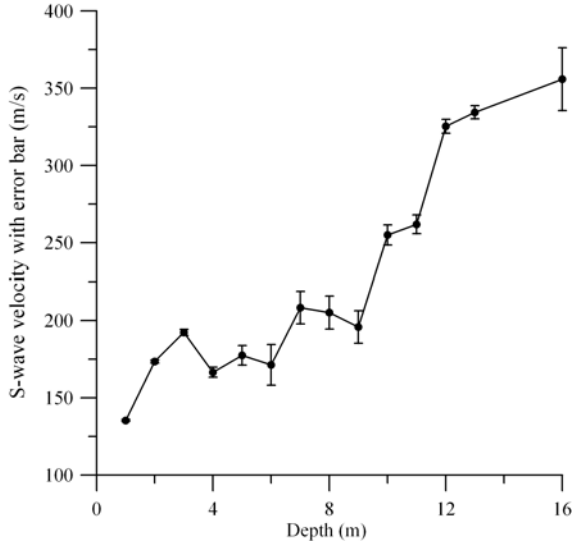

Figure 5. Inverted results of the San Jose example with an extra iteration from the inverted model of "Selected data" (Figure 3). Error bars were computed with the optimal damping vector (Table 4).

EDITED REFERENCES

Note: This reference list is a copy-edited version of the reference list submitted by the author. Reference lists for the 2008 SEG Technical Program Expanded Abstracts have been copy edited so that references provided with the online metadata for each paper will achieve a high degree of linking to cited sources that appear on the Web.

REFERENCES

Aki, K., and P. G. Richards, 1980, Quantitative seismology: W. H. Freeman.

Beaty, K. S., D. R. Schmitt, and M. Sacchi, 2002, Simulated annealing inversion of multimode Rayleigh wave dispersion curves for geological structure: Geophysical Journal International, **151**, 622–631.

Calderón-Macías, C., and B. Luke, 2007, Addressing nonuniqueness in inversion of Rayleigh-wave data for shallow profiles containing stiff layers: Geophysics, **72**, U1–U10.

Dorman, J., and M. Ewing, 1962, Numerical inversion of seismic surface wave dispersion data and crust-mantle structure in the New York-Pennsylvania area: Journal of Geophysical Research, **67**, 5227–5241.

Golub, G. H., and C. Reinsch, 1970, Singular value decomposition and least-squares solution: Numerical Mathematics, **14**, 403–420.

Ivanov, J., R. D. Miller, J. Xia, D. W. Steeples, and C. B. Park, 2006, Joint analysis of refractions with surface waves: An inverse solution to the refraction-traveltime problem: Geophysics, **71**, R131–R138.

Liang, Q., C. Chen, C. Zeng, Y. Luo, and Y. Xu, Inversion stability analysis of multimode Rayleigh-wave dispersion curves using low-velocity-layer models: Near Surface Geophysics, in press.

Lu, L., C. Wang, and B. Zhang, 2007, Inversion of multimode Rayleigh waves in the presence of a low-velocity layer: numerical and laboratory study: Geophysical Journal International, **168**, 1235–1246.

Luo, Y., J. Xia, J. Liu, Q. Liu, and S. Xu, 2007, Joint inversion of high-frequency surface waves with fundamental and higher modes: Journal of Applied Geophysics, **62**, 375–384.

Marquardt, D. W., 1965, An algorithm for least squares estimation of nonlinear parameters: Journal of the Society for Industrial and Applied Mathematics, **2**, 431–441.

Menke, W., 1984, Geophysical data analysis—Discrete inversion theory: Academic Press, Inc.

Miller, R. D., J. Xia, C. B. Park, and J. Ivanov, 1999, Multichannel analysis of surface waves to map bedrock: The Leading Edge, **18**, 1392–1396.

Minster, J. F., T. J. Jordan, P. Molnar, and E. Haines, 1974, Numerical modeling of instantaneous plate tectonics: Geophysical Journal of the Royal Astronomy Society, **36**, 541–576.

Song, Y. Y., J. P. Castagna, R. A. Black, and R. W. Knapp, 1989, Sensitivity of near-surface shear-wave velocity determination from Rayleigh and Love waves: 59th Annual International Meeting, SEG, Expanded Abstracts, 509–512.

Wiggins, R. A., 1972, The general linear inverse problem: Implication of surface waves and free oscillations for Earth structure: Review of Geophysical Space Physics, **10**, 251–285.

Xia, J., C. Chen, P. H. Li, and M. J. Lewis, 2004, Delineation of a collapse feature in a noisy environment using a multichannel surface wave technique: Geotechnique, **54**, 17–27.

Xia, J., W. E. Doll, R. D. Miller, T. J. Gamey, and A. M. Emond, 2005, A moving hum filter to suppress rotor noise in high-resolution airborne magnetic data: Geophysics, **70**, G69–G76.

Xia, J., R. D. Miller, and C. B. Park, 1999, Estimation of near-surface shear-wave velocity by inversion of Rayleigh wave: Geophysics, **64**, 691–700.

Xia, J., R. D. Miller, C. B. Park, J. A. Hunter, J. B. Harris, and J. Ivanov, 2002a, Comparing shear-wave velocity profiles from multichannel analysis of surface wave with borehole measurements: Soil Dynamics and Earthquake Engineering, **22**, 181–190.

Xia, J., R. D. Miller, C. B. Park, and G. Tian, 2002b, Determining Q of near-surface materials from Rayleigh waves: Journal of Applied Geophysics, **51**, 121–129.

———2003, Inversion of high-frequency surface waves with fundamental and higher modes: Journal of Applied Geophysics, **52**, 45–57.

Xia, J., R. D. Miller, C. B. Park, E. Wightman, and R. Nigbor, 2002c, A pitfall in shallow shear-wave refraction surveying: Journal of Applied Geophysics, **51**, 1–9.

Xia, J., Y. Xu, R. D. Miller, and C. Chen, 2006, Estimation of elastic moduli in a compressible Gibson half-space by inverting Rayleigh wave phase velocity: Surveys in Geophysics, **27**, 1–17.